Desalination and Water Treatment
www.deswater.com
doi: 10.5004/dwt.2020.24799

173 (2020) 105–116
January

Improving the performance of solar still by using nanofluids, vacuuming, and optimal basin water thickness

Khaled M. Bataineh*, Mohammad Abu Abbas

Department of Mechanical Engineering, Jordan University of Science and Technology, Irbid-Jordan, Tel. +962 2 7201000 Ext. 22383; Fax: +962 2 7201074; emails: k.bataineh@just.edu.jo (K.M. Bataineh), moabuabbas16@eng.just.edu.jo (M.A. Abbas)

Received 18 March 2019; Accepted 20 August 2019

ABSTRACT

This study presents theoretical and experimental investigations of the thermal behavior of solar still with added Al_2O_3 and SiO_2 nanoparticles for productivity enhancement. The investigations have been done during the summertime of 2018 in Irbid, Jordan (weather (32° N Latitude and 35° E Longitude). Accurate mathematical model has been developed based on balance equations. The numerical method is used to solve the nonlinear system of differential equations. The present numerical model is validated against experimental setup and found in a very good agreement. Accurate theoretical analyses allow a deeper understanding of the complex thermal behavior of solar still with added nanoparticles. Nanofluid temperature, glass temperature, heat transfer coefficients (HTC), and productivity of the solar have been analyzed. The effect of different Al_2O_3 and Si_2O_3 nanoparticle concentrations, basin water depth, and applying vacuum on daily water output has been analyzed. The results of this study show that utilizing Al_2O_3 and SiO_2 nanoparticles boosted the distilled water by 10% and 8.5%, respectively, at 0.5 cm depth of water and 0.2% nanoparticles concentration. Moreover, the productivity increases about 13% and 12% by adding Al_2O_3 and SiO_2 nanoparticles, respectively, when applying vacuum inside still at 2.5 cm depth of water.

Keywords: Solar still; Water distillation; Al_2O_3 and SiO_2 nanoparticles

1. Introduction

Production of fresh water is still a major challenge in several world regions, especially in remote areas. The percentage of fresh water available is about 3% of the world total water. Unfortunately, the worldwide distribution of freshwater reservoirs is irregular. Demand for freshwater has risen due to the combination of several factors; population growth, economic development, accelerated urbanization, and improvements in the living standard. Northern Africa and Western Asia countries (MENA) have the most serious water scarcity problem [1]. Desalination systems are considered a dependable strategy to provide fresh water in such regions. Due to these facts, research in desalination has gained interest in such regions. Recent advances in water desalination can be found in the literature [2,3].

Conventional desalination technologies that depend on the conventional forms of energy are becoming a serious issue as the world witnesses a significant increase in freshwater demand, also the fact that the fossil fuel resources in the world are finite. Moreover, conventional techniques require resources of electric power, complicated piping systems which usually are not available in remote areas. Therefore, it is important to find alternative desalination processes that do not basically depend on grid connection. Desalination technologies driven by solar energy systems are a good choice in regions which have high levels of solar radiation.

The performance of solar still depends on several factors such as climatic conditions (solar radiation intensity, ambient temperature, and wind speed), condensation surface

* Corresponding author.

1944-3994/1944-3986 © 2020 Desalination Publications. All rights reserved.

inclination, insulation type and thickness, solar still geometry, the orientation of still and depth of salty water. The yield of single slope solar still is low, reaching 1.5–4 L/m^2. Enhancing the productivity of such systems has received attention by many researchers [4–12]. Increasing basin water temperature and lowering the condensation glass cover temperature are the two main approaches to improve productivity. It is found that the average daily output increases with increasing solar radiation [4–6]. Moreover, increasing the basin water temperature also increases the distillate water yield [7–9].

The thickness of insulation and insulation material has a significant effect on solar still [10]. The insulation materials used in the solar still device are wood, thermocol, polyurethane, sawdust, and gypsum. Moreover, the productivity of solar still can be enhanced by utilizing external heating energy resource. It was found that continuous flowing of waste hot water along with the basin water has a significant effect during the night, while it is not effective during the sunshine hours [9]. Also, the inclination of the condensation surface has a significant effect on the productivity of solar still. Based on the latitude angle of solar still location, it is found that inclination of condensation surface should be designed at a particular inclined angle to get maximum productivity [11]. Moreover, it was found that the productivity of solar still increases with decrease in water depth [12–15]. Furthermore, wind speed has a positive effect on the productivity of the solar still. This due to the fact that increasing wind speed leads to increase convective heat losses at the condensation surface which results in decreasing temperature of the glass cover plate. It was found that productivity of solar still increases with the increase of wind speed up to a particular value beyond which the increase in wind speed becomes inefficient [16]. Bhardwaj et al. [17] studied the effect of using an external fan to decrease condensation temperature. They found out that the productivity of solar still increased from 0.020 to 0.100 kg. This increase was due to a decrease in condensation surface temperature from 42°C to 13°C. Moreover, it was found that utilizing internal and external reflectors with particular sloped angle can improve the performance and efficiency of solar still [18].

The performance of solar still can be improved by adding different types of nanofluids to basin water with different nanomaterial concentrations [19–24]. Utilizing nano fluid enhances the thermophysical properties of basin water. The added nanoparticles enhance the heat transfer rate [25]. Adding nanoparticles to the basin water improves the evaporation rate of solar still. Kabeel et al. [19] studied the effect of utilizing cuprous oxides nanomaterial on the basin liner of solar still. Their results showed that the cuprous oxides nanoparticles increased the water distillate by 16% and 25% as compared with the conventional still at weight concentration from 10% and 40%, respectively. Elango et al. [20] studied the effect of adding zinc oxide (ZnO) and tin oxide (SnO_2) nanoparticles with 0.1 volume concentrations. It was concluded that utilizing zinc oxide and tin oxide nanofluids increase productivity by 12.67% and 18.63%, respectively, compared to conventional solar still. Sahota and Tiwari [21] used mathematical models to study the effect of adding alumina nanoparticles in the water for a different mass of water and different volume concentration. They found that using alumina nanoparticles enhanced productivity about 8.9%, 10% and 12.2% with volume concentration 0.04%, 0.08% and 0.12%, respectively. Nazari et al. [22] conducted an experimental study to evaluate the effect of adding copper oxide nanoparticle with 0.08% volume concentration and integrating thermoelectric cooling channel on solar still productivity. The results illustrated that the productivity of solar still increased by about 81% compared with conventional still. Abdelal and Taamneh [23] conducted a set of experiments to improve the efficiency of solar distillation using a different type of nanoparticles integrated with the absorber plate. The results showed that the solar still efficiency increased by 109% and 65% when using 5% and 2.5% weight fraction of carbon nanotubes, and 30% when incorporating graphite nanotube with 2.5% weight fraction.

The behaviors of nanoparticles in solar still systems are not well understood yet, because most of the research conducted in this field is carried out using the experimental technique. There are few studies reported in the literature using mathematical techniques to analyze the effect of nanoparticles. The main objective of this study is to theoretically investigate the performance of solar still by adding aluminum oxide and silica oxide nanomaterials on the salty water of solar still under Jordan climatic conditions. The accurate mathematical model allows a deeper understanding of the main involved physical processes. Furthermore, it allows a rigorous optimization study for the current problem. More specifically, the developed mathematical model will be used to estimate the basin nanofluid temperature, glass cover temperature, heat transfer coefficients (HTCs) and daily water distilled of the proposed solar still. Experimental models are built to validate the developed mathematical model. The effect of several key factors that affect the solar still daily productivity is numerically and experimentally investigated. The major factors studied are nanoparticles concentrations, basin water depth, and the effect of vacuum inside solar still. The actual contribution of this article is providing accurate theoretical models for solar still under the combined actions of several measures to improve the performance. Previous studies have focused on one measure for improving performance.

2. Theoretical modeling

This section describes the development of the mathematical model for the solar still with added nanoparticles on the base fluid. This model is used to determine the hourly distilled water productivity and the daily efficiency of the solar still. Solar still as shown in Fig. 1 mainly consists of a condensation glass cover, basin liner water, and collecting channels. Collecting evaporated water (distilled) by condensing it on a cool sloping surface is the basic working principle of the solar still. The condensation cover could be single sloped or pyramidal. The salty water in the black painted basin liner is heated by the transmitted solar radiation that has been absorbed by the basin liner. In this technique, the basin and the salty water act as an evaporator, while the glass surface acts as a condenser. The bottom and all side walls of the basin liner are well insulated. The technical specifications of the solar still and operational parameters are summarized in Table 1.

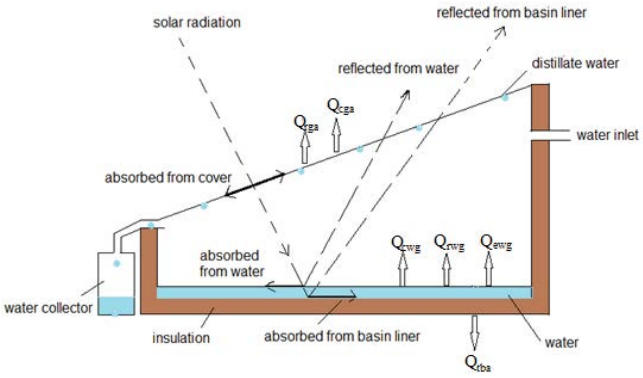

Fig. 1. Schematic diagram of single slope solar still.

Table 1
Specifications of the solar still

Solar still part	Specification
Basin	$\alpha_b = 0.90$
	A_b (m²) = 0.36
	cp_b (J/kg) = 460
Glass	Glass thickness (m) = 0.004
	$\alpha_g = 0.05$
	$\tau_g = 0.85$
	$\varepsilon_g = 0.88$
	A_g (m²) = 0.4
	cp_g (J/kg K) = 840
	ρ_g (kg/m³) = 2,500
	m (kg) = 10
Basefluid	$\alpha_w = 0.05$
	$\tau_w = 0.9$
	$\varepsilon_w = 0.96$
	A_w (m²) = 0.36
	hfg_w (J/kg K) = 2,35,0000
Aluminum nanoparticles	ρ (kg/m³) = 3,960
	cp (J/kg) = 773
	K (w/m k) = 41
	$B = 8.1 \times 10^{-6}$
Silica nanoparticles	ρ (kg/m³) = 2,620
	cp (J/kg) = 900
	K (w/m k) = 1.4
	$B = 5.6 \times 10^{-7}$

The main energy balance equations for basin liner, basin nanofluid, and glass cover can be summarized as follows; the energy balance for the solar still system is as follows:

$$\sum Q_{in} = \sum Q_{out} \tag{1}$$

A fraction of solar radiation falling on basin liner of solar still is absorbed. The absorbed energy is stored in the basin liner and the remaining is transmitted by convection to basin nanofluid, the rest is rejected from basin liner to surrounding by conduction through the bottom of the solar still. The transient energy balance equation for the basin liner is given as [26]:

$$I_t A_b \alpha_b \tau_g \tau_{nf} = m_b cp_b \frac{dT_b}{dt} + Q_{cb-nf} + Q_{loss-ba} \tag{2}$$

The basin nanofluid received heat from the absorbed fraction of striking solar radiation and the heat transmitted from basin liner by convection. The gained energy is stored in nanofluid due to its specific heat and rest of the energy is released from nanofluid surface to the glass cover by evaporation, convection, and radiation. The transient energy balance equation for the basin nanofluid is given as [26,27]:

$$I_t A_{nf} \alpha_{nf} \tau_g + Q_{cb-nf} = m_{nf} cp_{nf} \frac{dT_{nf}}{dt} + Q_{cnf-g} + Q_{enf-g} + Q_{rnf-g} + Q_{mw} \tag{3}$$

The glass cover gains heat from both the absorbed fraction of solar radiation and heat transmitted from basin nanofluid surface by evaporation convection and radiation. Part of the gained heat is stored in the glass cover while the rest is lost through convection and radiation to the ambient. Energy balance for the glass cover is given as [27]:

$$I_t A_g \alpha_g + Q_{cnf-g} + Q_{enf-g} + Q_{rnf-g} = m_g cp_g \frac{dT_g}{dt} + Q_{rg-sk} + Q_{cg-a} \tag{4}$$

The convective heat transfer between basin liner and nanofluid is given as [28,29]:

$$Q_{cb-nf} = h_{cb-nf} A_b (T_b - T_{nf}) \tag{5}$$

The convective HTC between basin liner and nanofluid, $h_{cb\text{-}nf}$, is given as [21]:

$$h_{cb-nf} = Nu \frac{K_{nf}}{\delta} \tag{6}$$

The Nusselt number is calculated as [21]:

$$Nu = 0.54 (Gr \cdot Pr)^{0.25} \tag{7}$$

The Grashof and Prandtl number is calculated as [21]:

$$Gr = \left(\frac{gB(T_b - T_{nf})\rho_{nf}^2 \delta^3}{\mu_{nf}^2} \right) \tag{8}$$

$$Pr = \left(\frac{\mu_{nf} cp_{nf}}{K_{nf}} \right) \tag{9}$$

The heat releases by conduction through the basin liner to the atmosphere are given by [30]:

$$Q_{loss-ba} = \frac{K_i}{L_i} A_b (T_b - T_a) \tag{10}$$

where K_i and L_i are thermal conductivity and thickness of insulation. The convective heat transfer between nanofluid and glass cover is given by [28,29]:

$$Q_{\text{cnf}-g} = h_{\text{cnf}-g} A_{\text{nf}} (T_{\text{nf}} - T_g) \tag{11}$$

where the convective HTC between nanofluid and glass cover, $h_{\text{cnf}-g}$, is given by [31]:

$$h_{\text{cnf}-g} = 0.884 A_{\text{nf}} \left((T_{\text{nf}} - T_g) + \frac{(P_{\text{nf}} - P_g)(T_{\text{nf}} + 273.15)}{26,8900 - P_{\text{nf}}} \right)^{\frac{1}{3}} \tag{12}$$

where P_w and P_g are the partial pressure of the nanofluid and glass cover, respectively, given as [32]:

$$P_{\text{nf}} = \text{EXP}\left(25.317 - \frac{5,144}{(T_{\text{nf}} + 273.15)} \right) \tag{13}$$

$$P_g = \text{EXP}\left(25.317 - \frac{5,144}{(T_g + 273.15)} \right) \tag{14}$$

The radiative heat transfer between nanofluid and glass cover is given by [27]:

$$Q_{\text{rnf}-g} = \sigma . \varepsilon_{\text{eff}} A_{\text{nf}} \left((T_{\text{nf}} + 273.15)^4 - (T_g + 273.15)^4 \right) \tag{15}$$

where ε_{eff} is the nanofluid-glass effective emissivity given as [32]:

$$\varepsilon_{\text{eff}} = \left(\frac{1}{\left(\frac{1}{\varepsilon_{\text{nf}}} + \frac{1}{\varepsilon_g} - 1 \right)} \right) \tag{16}$$

The evaporative heat transfer between nanofluid and glass cover is given by [28,29]:

$$Q_{\text{enf}-g} = h_{\text{enf}-g} A_{\text{nf}} (T_{\text{nf}} - T_g) \tag{17}$$

where the evaporative HTC between nanofluid and glass cover, $h_{\text{enf}-g}$, is given by [28,29]:

$$h_{\text{enf}-g} = \frac{0.0162 h_{\text{cnf}-g} (P_{\text{nf}} - P_g)}{(T_{\text{nf}} - T_g)} \tag{18}$$

The makeup water is heated as following [33]:

$$Q_{\text{mw}} = m' \left(\text{cp}_w \cdot T_w - \text{cp}_a \cdot T_a \right) \tag{19}$$

The radiative heat transfer between glass and sky is given by [28,29]:

$$Q_{\text{rg}-\text{sk}} = h_{\text{rg}-\text{sk}} A_g (T_g - T_{\text{sk}}) \tag{20}$$

where the radiative HTC between glass cover and sky, $h_{\text{rg}-\text{sk}}$, is given by [28,29]:

$$h_{\text{rg}-\text{sk}} = \sigma \varepsilon_g A_g \left(\frac{\left((T_g + 273.15)^4 - (T_{\text{sk}} + 273.15)^4 \right)}{\left(T_g - T_a \right)} \right) \tag{21}$$

The sky temperature is given as [31]:

$$T_{\text{sk}} = T_a - 6.0 \tag{22}$$

The convective heat transfer between the glass cover and ambient air, $Q_{\text{cg}-a}$ is given by [34]:

$$Q_{\text{cg}-a} = h_{\text{cg}-a} A_g (T_g - T_a) \tag{23}$$

where the convective HTC between glass cover and ambient, $h_{\text{cg}-a}$, is taken from [32]:

$$h_{\text{cg}-a} = 2.8 + 3V \tag{24}$$

The hourly yield is given as [32]:

$$m' = \frac{h_{\text{enf}-g} A_{\text{nf}} (T_{\text{nf}} - T_g) \times 3,600}{hfg} \tag{25}$$

The daily efficiency of solar still is given by [34]:

$$\eta = \frac{\sum m' \cdot hfg}{\sum A_g I_t} \tag{26}$$

The density of nanofluids (ρ_{nf}) is determined as [35]:

$$\rho_{\text{nf}} = \left(1 - Q_v \right) \rho_{\text{bf}} + Q_v \rho_p \tag{27}$$

The specific heat of the nanofluid (cp_{nf}) is calculated using [36]:

$$\text{cp}_{\text{nf}} = \frac{\left(1 - Q_v \right) (\rho \text{cp})_{\text{bf}} + Q_v (\rho \text{cp})_p}{\rho_{\text{nf}}} \tag{28}$$

The viscosity of the nanofluid (μ_{nf}) can also be determined using [37]:

$$\mu_{\text{nf}} = \mu_{\text{bf}} \left(1 + 2.5 Q_v \right) \tag{29}$$

The effective thermal conductivity of nanofluids (K_{nf}) can also be evaluated using [38]:

$$\frac{K_{\text{nf}}}{K_{\text{bf}}} = \frac{K_p + 2K_{\text{bf}} + 2Q_v \left(K_p - K_{\text{bf}} \right)}{K_p + 2K_{\text{bf}} - Q_v \left(K_p - K_{\text{bf}} \right)} \tag{30}$$

The effective thermal expansion of nanofluids (B_{nf}) can also be evaluated using [39]:

$$B_{\text{nf}} = \left(1 - Q_v \right) B_{\text{bf}} + \left(Q_v \times B_p \right) \tag{31}$$

The specific heat of the basefluid (cp_{bf}) is calculated using [40]:

$$cp_{bf} = 4.217 - 0.0056T_{bf} + 0.00129T_{bf}^{1.5} - 0.000115T_{bf}^{2} + 4.149\times10^{-6}T_{bf}^{2.5} \quad (32)$$

The density of basefluids (ρ_{bf}) is determined as [40]:

$$\rho_{bf} = 999.79 + 0.0683T_{bf} - 0.0107T_{bf}^{2} + 0.00082T_{bf}^{2} - 2.303\times10^{-5}T_{bf}^{3} \quad (33)$$

The effective thermal conductivity of basefluids (K_{bf}) can also be evaluated using [40]:

$$K_{bf} = 0.565 + 0.00263T_{bf} - 0.00015T_{bf}^{1.5} - 1.515\times10^{-6}T_{bf}^{2} - 0.00094T_{bf}^{0.5} \quad (34)$$

The viscosity of the basefluid (μ_{bf}) can also be determined using [41]:

$$\mu_{bf} = 2.414\times10^{-5}\times10^{\frac{247.8}{(T_{bf}+273)-140}} \quad (35)$$

The advantage of having vacuum/low pressure inside the solar still is preventing or reducing heat transfer between water and glass cover by convection. Therefore, the heat loss from the water to the glass cover is only due to radiation and evaporation (h_{cwg} = 0). So that the evaporation HTC is calculated using the thermal balance equation at the glass cover [42]:

$$h_{ewg} = \frac{\left(h_{cga}+h_{rga}\right)\left(T_g - T_a\right)}{\left(T_{nf} - T_g\right)} - \left(h_{rwg}\right) \quad (36)$$

3. Experimental setup

In order to validate our theoretical model, prototype model according to Table 1 is built. The solar still is placed in Jordan University of Science and Technology, Jordan (32° 28′ 26.39 N latitude and 35° 59′ 3.59 E longitude).

4. Numerical solution

The previously derived mathematical model was numerically solved to investigate the effect of adding aluminum oxide and silica oxide nanoparticles on basefluid of solar still. The system of nonlinear differential equations for the thermal model described previously contains three variables and three derivatives (Eqs. (2)–(4)). The best method for solving this system of equations is Runge-Kutta forth order method known as rk4. These equations can be formulated as an initial value problem. The initial values of the variables are known and the integration is performed with time step equal to 1 s. The unknown variables T_b, T_g, T_{nf}, h_{enf-g}, h_{rnf-g}, h_{cnf-g} and the quantity of distilled water productivity were evaluated per hour. Initial conditions corresponding to the main temperatures of the solar still were assumed to be equal to that of the ambient temperature at 8 am. Meteorological conditions (solar radiation, ambient temperature, and wind velocity) and their variation throughout the test day are introduced in the model as boundary conditions. Amount of water inside the solar still and nanoparticles concentration was assumed to remain constant. Using these values of temperatures; different HTCs from nanofluid to condensation surface and from condensation surface to ambient were calculated for a time interval (t = 1 s.) as stated in the program. The flow chart of the numerical solution is shown in Fig. 2.

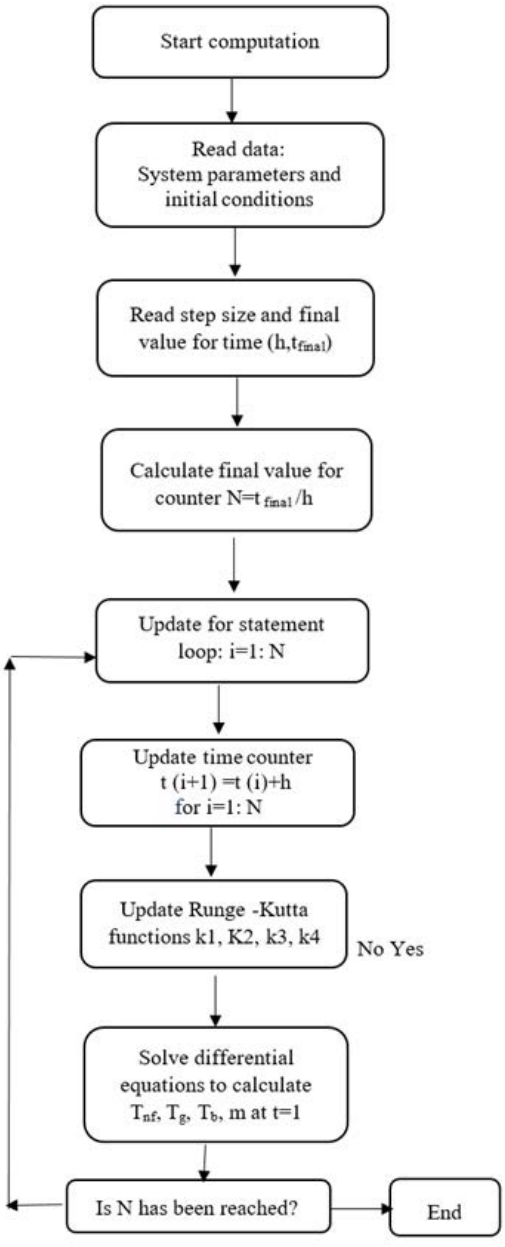

Fig. 2. System flow chart.

5. Results and discussions

5.1. Climatological conditions

Table 2 lists the measured global solar intensity and ambient temperature for several days of summer season under Jordan weather conditions for the year 2018. It can be observed that the maximum value of solar intensity is reached at mid noon and thereafter it begins to decrease up to the evening, whereas the ambient air temperature has reached the maximum value at 3:00 pm. The maximum value of solar intensity is attained faster than the maximum value of ambient air temperature mainly due to more thermal capacity of ambient air.

5.2. Model verification

The present mathematical work is compared against experimental work. A prototype according to specifications listed in Table 1 is built. The experimental study has been carried out during a period of 8 am until 12 am. Figs. 3a–c and Figs. 4a–c compare between present theoretical predictions and experimental output at different nanoparticle concentrations. It is clear from the curves presented in Figs. 3 and 4 that there are excellent matches between theoretical and experimental work. Fig. 5 shows that the maximum error percentage between the theoretical and experimental is less than 6.5%. Also, as shown in Fig. 6 the increase in efficiency

Table 2
Hourly variation of global solar intensity and ambient temperature in 24/7/2018 and 26/7/2018

Time (h)	Solar radiation (W)	Ambient temperature (°C)	Solar radiation (W)	Ambient temperature (°C)
	24/7/2018		26/7/2018	
8	191.9	24.84	206.28	23.91
9	397.72	28.73	418.45	25.9
10	604.56	31.1	628.63	28.01
11	780.64	32.88	798.69	29.87
12	899.32	34.31	961.88	31.2
1	949.3	34.89	965.68	32.49
2	928.77	35.54	936	33.35
3	835.79	35.68	848.35	33.93
4	685.08	35.69	697.5	33.9
5	498.55	35.36	517	32.83
6	286.56	34.08	304	31.54
	5/8/2018		30/6/2018	
8	206	25.28	200	23.61
9	418	28.19	413	25.79
10	626	30	618	28.57
11	798	32.52	786	31.55
12	961	33.58	902	32.99
1	965	34.02	963	34.32
2	935	34.44	940	34.82
3	848	34.71	845	35
4	697	34.65	706	35.09
5	517	34.01	513	33.92
6	303	33.04	298	32.17
	5/7/2018		19/7/2018	
8	203.88	21.54	229.59	21.52
9	437.96	24.32	464	23.51
10	666.55	26.28	645	24.95
11	854.82	28.82	774	26.01
12	969.8	30.66	863	26.99
1	1,019.34	32.14	981	28.39
2	995.21	33.11	953	29.13
3	903.03	33.48	869	29.38
4	746.88	33.52	726	29.36
5	538.5	32.66	532	28.91
6	302.24	31.33	313	28.32

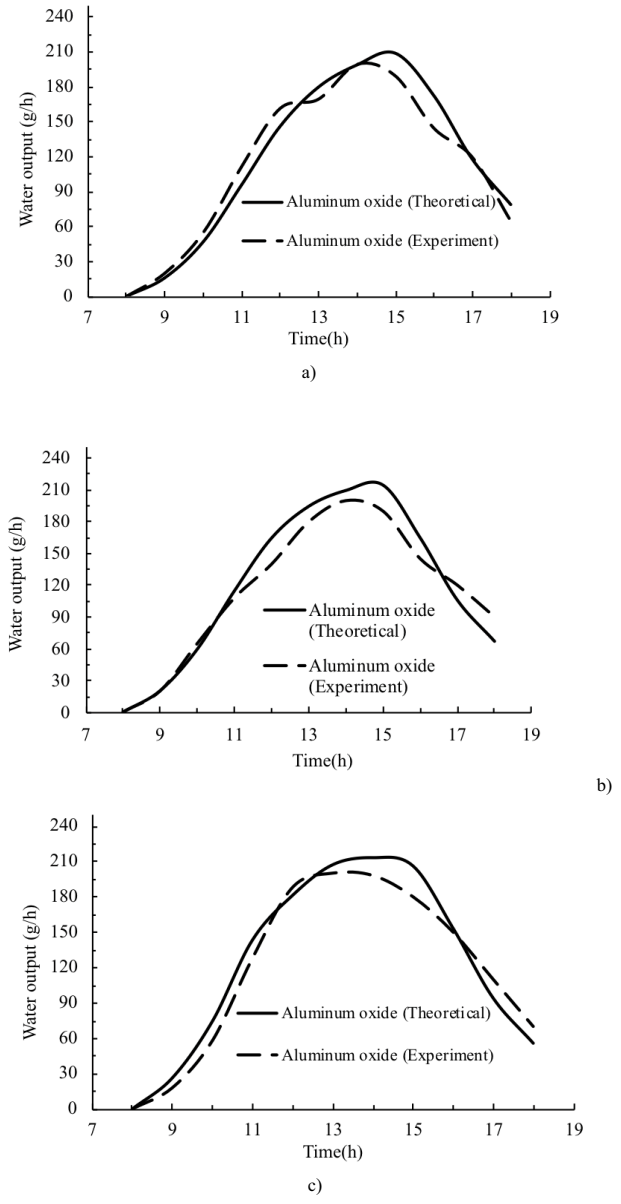

Fig. 3. Comparison between theoretical model predictions and experimental measurements with added Al_2O_3 nanoparticles at (a) 0.2%, (b) 0.4% and (c) 0.6%.

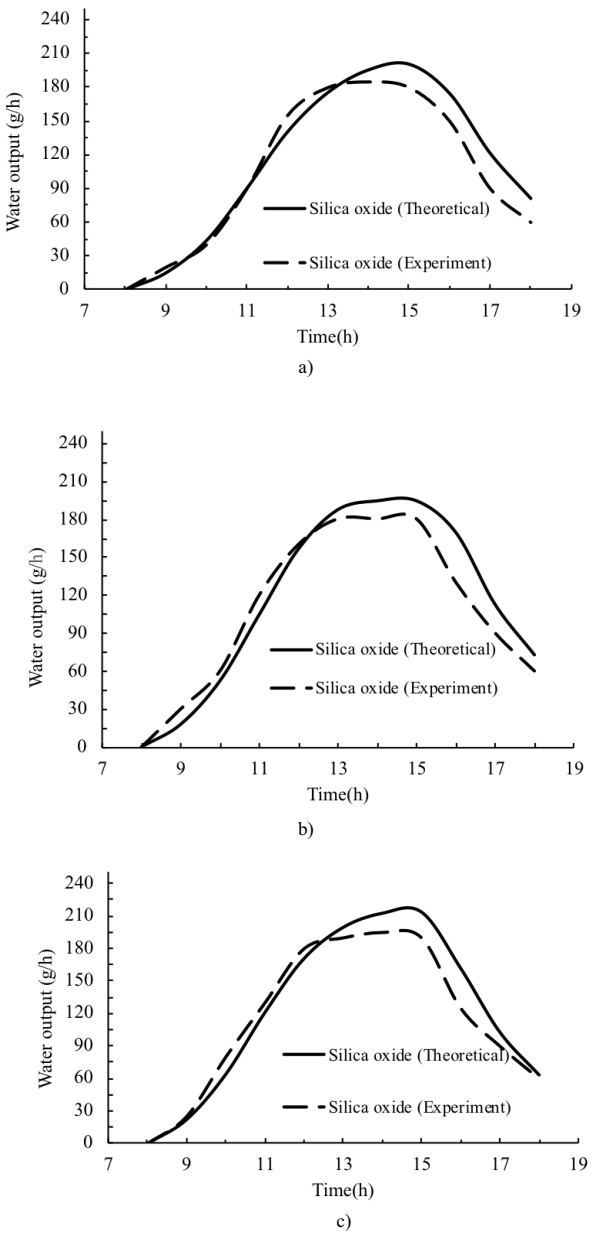

Fig. 4. Comparison between theoretical model predictions and experimental measurements with added SiO_2 nanoparticles at (a) 0.2%, (b) 0.4% and (c) 0.6%.

between the two work during sunlight period was very close, where the maximum increase efficiency was 11.7% and 14% at 0.6% nanoparticle concentration when adding aluminum oxide for experimental study and theoretical work, respectively, and 10.3 and 11.7 at 0.6% nanoparticle concentration when adding silica oxide for experimental and theoretical work, respectively.

Figs. 7a and b represent hourly variations of distilled water output of solar still with added aluminum oxide and silica oxide, respectively, for several nanoparticles concentrations levels. The theoretical results indicate that an increase in the nanoparticle concentration leading to an increase in the still yield during a period from 8 am until 3 pm and a sharp reduction in the still yield after 3 pm. The reason behind this may be that, when adding nanoparticles material on salty water, the specific heat of nanofluid decreases so that, the basin water temperature can reach high values which leads to higher evaporation rate. On the other hand, after 3 pm, when solar radiation level starts decreasing, due to lower values of specific heat of the basin water with nanoparticles, the temperature of basin water decreases at higher rate leads to lower evaporation rate, which is responsible for decreasing in the solar still output.

Figs. 8a and b and Figs. 9a and b represent basin nanofluid temperature and condensation surface

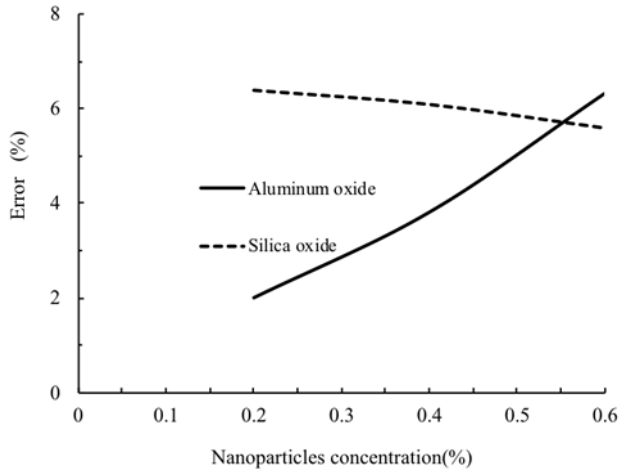

Fig. 5. Error of theoretical model predictions for added Al_2O_3 and SiO_2 nanoparticles at different concentrations.

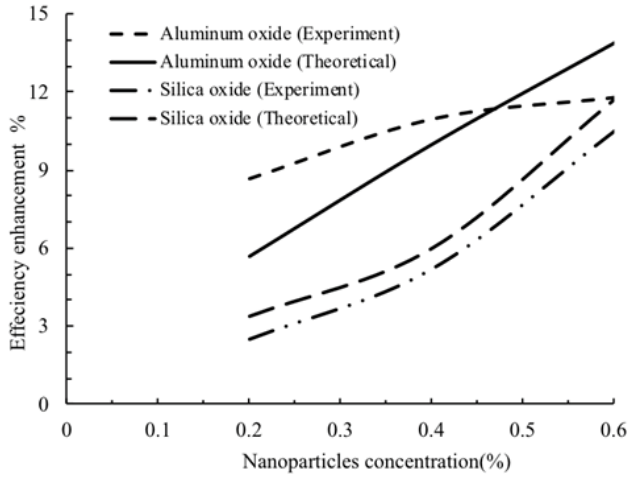

Fig. 6. Efficiency enhancement (in sunlight only) with added Al_2O_3 and SiO_2 nanoparticle at different concentrations.

temperature when adding silica oxide and aluminum oxide, respectively. The results revealed that the trend of the hourly variation of nanofluid temperature and condensation surface temperature curves are similar to that of hourly variations of still productivity curve due to the reason mentioned above.

5.3. Effect of nanomaterial concentrations on daily water output:

The daily yield of solar distillation system when adding nanoparticles at different concentrations is evaluated theoretically as shown in Fig. 10. It can be observed that the productivity of the solar still increases with the increase of the concentration ratio of nanoparticles until a critical value beyond which its effect becomes insignificant. Where the maximum distilled water was 1,427 g/d

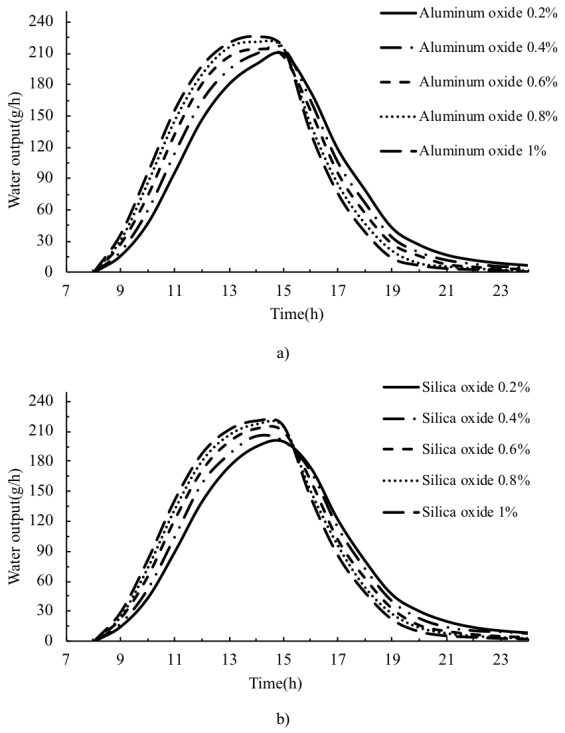

Fig. 7. Hourly water output at different concentration (0.2%–1%) for (a) aluminum oxide and (b) silica oxide.

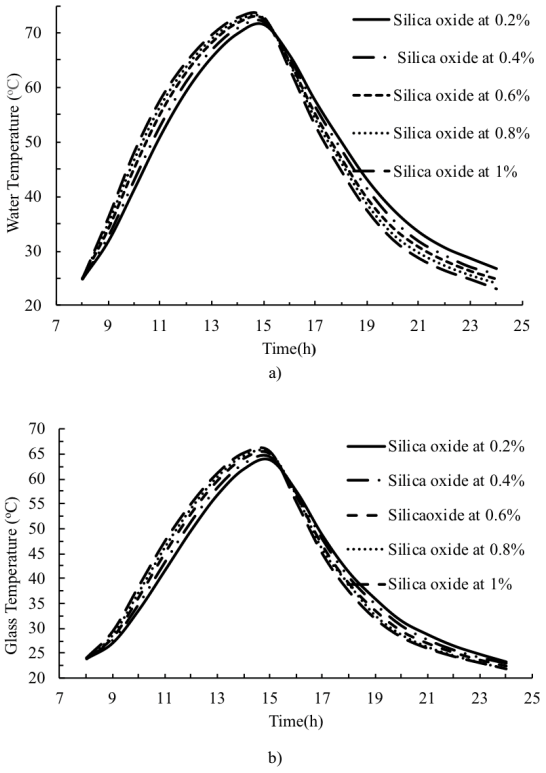

Fig. 8. Hourly variation of (a) water temperature and (b) glass temperature using SiO_2 at different nanoparticles concentrations.

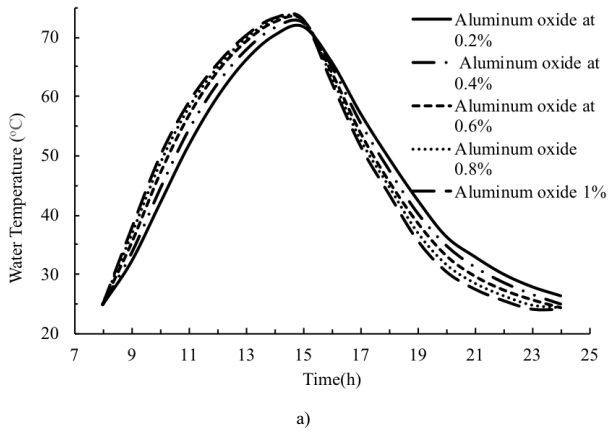

Fig. 9. Hourly variation of (a) water temperature and (b) glass temperature using Al_2O_3 at different nanoparticles concentrations.

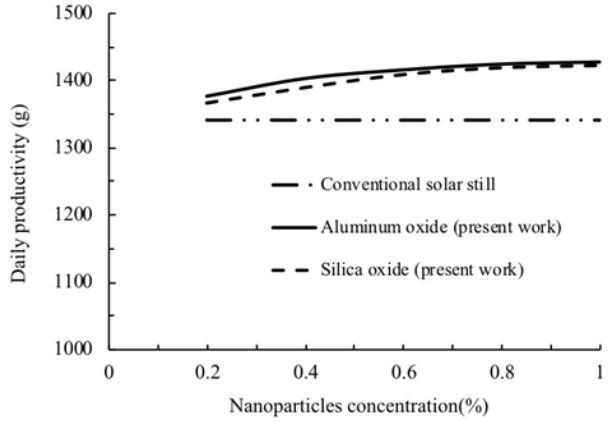

Fig. 10. Daily water output of solar still at different nanoparticles concentration.

and 1,422.2 at 1% concentration for aluminum oxide and silica oxide nanoparticle, respectively. On the other hand, the maximum water output for conventional still was 1,342.3 g/d.

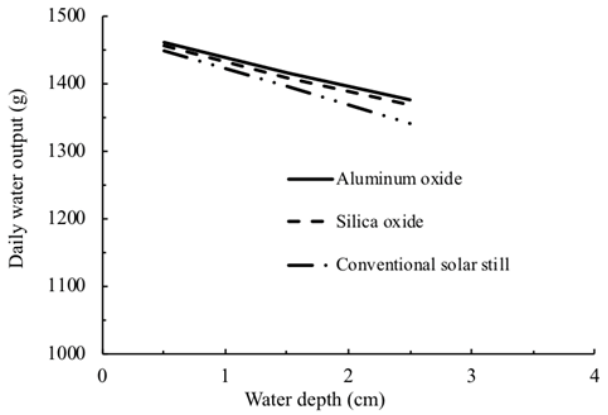

Fig. 11. Daily water output at a different basin water depth.

5.4. Effect of basin water depth

The effect of basin water depth on system productivity is numerically investigated. Fig. 11 depicts the effect of basin water depth on solar still productivity. The numerical investigations show that productivity is inversely linearly proportional to the water depth. This is due to the fact that small depth leads to higher basin water temperature which ultimately leads to a higher rate of evaporation. The cumulative water output was approximately 1,462 and 1,456 g/d for aluminum oxide and silica oxide, respectively and 1,448 g/d for conventional solar still at lowest water depth (0.5 cm). While for water depth = 2.5 cm, the daily water output was approximately 1,377 and 1,368 g/d for aluminum oxide and silica oxide, respectively, whereas for conventional solar still, it was 1,342 g/d.

Figs. 12a–c show the variation of hourly variations of basin water temperature and glass cover temperature with basin water depths for conventional solar still and solar still with added nanoparticles. It can be seen from curves presented in Fig. 12 that the basin water temperature and glass cover temperature increase significantly with a decrease in the water depth during a period from 8 am to 3 pm while the temperatures decrease after 3 pm. This can be explained as follows: the amount of water decreases with decreasing water depth allowing it to reach higher temperature during high values of radiation. After 3 pm, the incoming solar radiation starts decreasing and the basin water temperature starts dropping at a higher rate due to small heat capacity.

5.5. Effect of using vacuum on solar still yield

Fig. 13 shows the effect of using a vacuum inside the solar distillation system. It is observed that there is a high increase in daily water output from the solar still device when applying a vacuum inside the still. This is due to avoid heat transfer by convection from water to glass cover, therefore decrease losses, resulting in higher water temperature. In the conventional still, having a vacuum, increases the daily output to 1,432 g/d with the vacuum case, while the maximum daily water output when adding aluminum oxide and silica oxide in the vacuum case was 1,518 and 1,510 g/d, respectively, at 1% nanoparticle concentration.

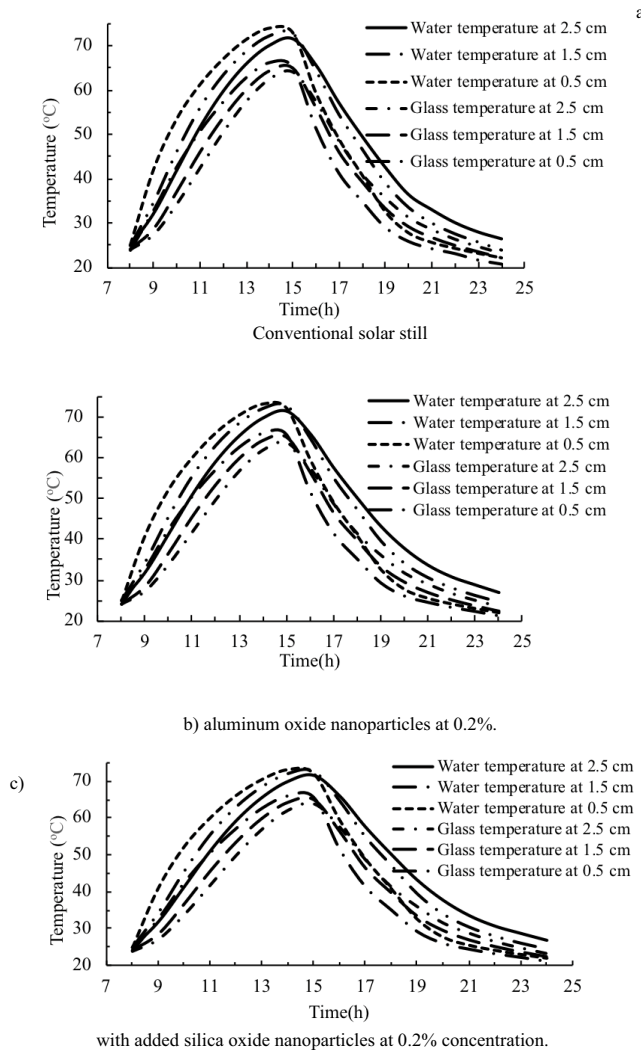

Fig. 12. Variations of water and glass cover temperature with water depth for (a) conventional solar still, (b) with added aluminum oxide nanoparticles at 0.2%, and (c) with added silica oxide nanoparticles at 0.2% concentration.

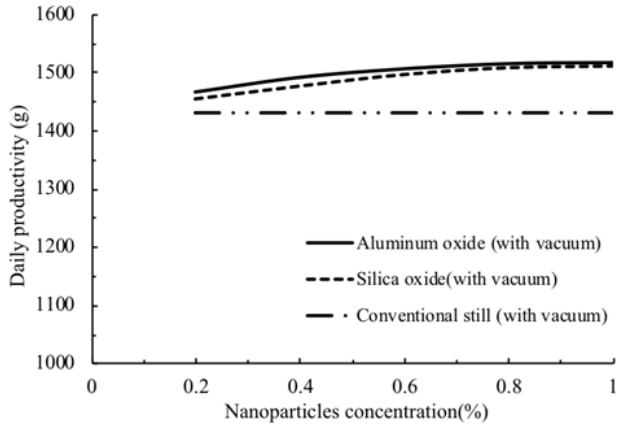

Fig. 13. Effect of applying vacuum inside solar still.

6. Conclusion

An accurate mathematical model for the thermal behavior of solar still utilizing nanoparticles is developed. The model was validated against experimental work and found in very good agreement. The nonlinear system of the differential equation is numerically solved for a deeper understanding of the thermal behavior of solar still. The effect of adding aluminum oxide and silica oxide nanoparticles with a different concentration on solar still productivity has been experimentally and numerically analyzed. Moreover, the effect of basin nanofluid depth of a solar still ranging from 0.5 to 2.5 cm was theoretically investigated. The effectiveness of applying vacuum inside still was evaluated. The results are summarized as follows:

- The productivity of solar still with nanoparticles increases during sunlight hours and decreases during moonlight hours.
- The productivity of the solar still increases with nanoparticles concentration until certain levels and it starts to level off.
- Utilizing nanoparticle alone, the increase is only limited up to 3%–6% at water depth 2.5 cm.
- The productivity of solar still is inversely proportional with basin nanofluid depth.
- Applying vacuum inside solar still, the productivity increases by 13% and 12% for aluminum oxide and silica oxide, respectively.

Symbols

A	—	Area, m^2
C_{pw}	—	Water specific heat, J/kg k
C_{pa}	—	Air specific heat, J/kg k
h	—	Heat transfer coefficient, W/m^2 k
h_{fg}	—	Enthalpy of evaporation, J/kg
I	—	Solar radiation, W
K_i	—	Thermal conductivity, W/m k
L_i	—	Thickness, m
m	—	Mass, kg
m'	—	Mass output, kg/s
P	—	Partial pressure, Pa
Pr	—	Prandtl number
Q	—	Heat transfer, W
Q_p	—	Nanoparticle concentration
Ra	—	Rayleigh number
t	—	Time, s
T	—	Temperature, °C
V	—	Wind speed, m/s

Greek symbols

ε	—	Emissivity
α	—	Absorptivity
τ	—	Transmissivity
ε_{eff}	—	Water–glass effective emissivity
B	—	Thermal expansion coefficient
ρ	—	Density, kg/m^2
σ	—	Stefan–Boltzmann constant, W/m^2 k^4
δ	—	Characteristic length, m

μ	—	Dynamic viscosity, N/m^2 s
g	—	Gravity acceleration, m/s^2
η	—	Daily efficiency of the still

Subscripts

α	—	Ambient
β	—	Basin liner
bf	—	Base fluid
c	—	Convection
e	—	Evaporative
g	—	Condensation glass
m_w	—	Make up water
n_f	—	Nanofluid
p	—	Nanoparticles
r	—	Radiative
sk	—	Sky
i	—	Insulation
W	—	Water
m_w	—	Make up water

References

[1] K. Bataineh, Multi-effect desalination plant combined with thermal compressor driven by steam generated by solar energy, Desalination, 385 (2016) 39–52.
[2] M.S. Khan, B. Lal, K.M. Sabil, I. Ahmed, Desalination of seawater through gas hydrate process: An overview, J. Adv. Res. Fluid Mech. Thermal Sci., 55 (2019) 65–73.
[3] A.A.S. Azmi, F.S. Sani, F. Ali, M. Mel, Interactive effect of temperature, pH and light intensity on biodesalination of seawater by synechococcus sp. PCC 7002 and on the cyanobacteria growth, J. Adv. Res. Fluid Mech. Thermal Sci., 52 (2018) 85–93.
[4] A.L. Ghoneyem, A. Ileri, Software to analyze solar stills and an experimental study on the effects of the cover, Desalination, 114 (1997) 37–44.
[5] O. Badran, M. Abu-Khader, Evaluating thermal performance of a single slope solar still, Heat Mass Transf., 43 (2007) 985–995.
[6] E.A. Almuhanna, Evaluation of single slop solar still integrated with evaporative cooling system for brackish water desalination, J. Agric. Sci., 6 (2014) 48–58.
[7] K.K. Murugavel, K.S.K. Chockalingam, K. Srithar, Modeling and verification of double slope single basin solar still using laboratory and actual solar conditions, Jordan J. Mech. Ind. Eng., 3 (2009) 228–235.
[8] A.Z. AlGarni, Enhancing the solar still using immersion type water heater productivity and the effect of external cooling fan in winter, Appl. Solar Energy, 48 (2012) 193–200.
[9] G.N. Tiwari, H.P. Madhuri, Effect of water flow over the glass cover of a single basin solar still with an intermittent flow of waste hot water in the basin, Energy Convers. Manage., 25 (1985) 315–322.
[10] B.B. Sahoo, N. Sahoo, P. Mahanta, L. Borbora, P. Kalita, U.K. Saha, Performance assessment of a solar still using blackened surface and thermocol insulation, Renew. Energy, 33 (2008) 1703–1708.
[11] B.A. Akash, M.S. Mohsen, W. Nayfeh, Experimental study of the basin type solar still under local climate conditions, Energy Convers. Manage., 41 (2000) 883–890.
[12] R. Tripathi, G.N. Tiwari, Effect of water depth on internal heat and mass transfer for active solar distillation system, Desalination, 170 (2004) 251–262.
[13] T. Rajesh, G.N. Tiwari, Thermal modeling of passive and active solar stills for different depths of water by using the concept of solar fraction, Sol. Energy, 80 (2006) 956–967.
[14] M.K. Phadatare, S.K. Verma, Influence of water depth on internal heat and mass transfer in a plastic solar still, Desalination, 217 (2007) 267–275.
[15] M.R. Rajamanickam, A. Ragupathy, Influence of water depth on internal heat and mass transfer in a double slope solar still, Energy Procedia, 14 (2012) 1701–1708.
[16] El-Sebaii, Effect of wind speed on active and passive solar stills, Energy Convers. Manage., 45 (2004) 1187–1204.
[17] R. Bhardwaj, M.V. Kortenaar, R.F. Mudde, Maximized production of water by increasing area of condensation surface for solar distillation, Appl. Energy, 154 (2015) 480–490.
[18] Abdul Jabbar N. Khalifa, Hussein A. Ibrahim, Effect of inclination of the external reflector on the performance of a basin type solar still at various seasons, Energy, Sustain. Dev., 13 (2009) 244–249.
[19] A.E. Kabeel, Z.M. Omara, F.A. Essa, A.S. Abdullah, T. Arunkumar, R. Sathyamurthy, Augmentation of a solar still distillate yield via absorber plate coated with black nanoparticles. Alexandria Eng. J., 56 (2017) 433–438.
[20] T. Elango, A. Kannan, K.K. Murugavel, Performance study on single basin single Slope solar still with different water nanofluids, Desalination, 360 (2015) 45–51.
[21] L. Sahota, G.N. Tiwari, Effect of Al_2O_3 nanoparticles on the performance of Passive double slope solar still, Sol. Energy, 130 (2016) 260–272.
[22] S. Nazari, H. Safarzadeh, M. Bahiraei, Performance improvement of a single slope solar still by employing thermoelectric cooling channel and copper oxide nanofluid: an experimental study, J. Cleaner Prod., 208 (2019) 1041–1052.
[23] N. Abdelal, Y. Taamneh, Enhancement of pyramid solar still productivity using absorber plates made of carbon fiber/CNT-modified epoxy composites, Desalination, 419 (2017) 117–124.
[24] B. Gupta, A. Kumar, P. Baredar, Experimental investigation on modified solar still using nanoparticles and water sprinkler attachment, Front. Mater.. 4 (2017) 1–7.
[25] A. Hilo, A. Abu Talib, S. Nfawa, M. Sultan, M. Hamid, M.I Bheekhun, Heat transfer and thermal conductivity enhancement using graphene nanofluid: a review, J. Adv. Res. Fluid Mech. Thermal Sci., 55 (2019) 74–87.
[26] V. Velmurugan,S. Pandiarajan, G. Valeo, L. Subramanian, C. Prabaharan, K. Srithar, Integrated performance of stepped and single basin solar stills with mini solar pond. Desalination, 249 (2009) 902–919.
[27] K. Murugavel, S. Sivakumar, J. Ahamed, Kn Chockalingam, K. Srithar, Single basin double slope solar still with minimum basin depth and energy storing materials, Appl. Energy, 87 (2010) 514–523.
[28] V. Velmurugan, K.J. Kumar KJ, T. NoorulHaq, K. Srithar, Performance analysis in stepped solar still for effluent desalination, Energy, 34 (2009) 1179–1186.
[29] V. Velmurugan, S. Kumaran, V. Prabhu, K. Srithar, Productivity enhancement of stepped solar still–performance analysis, Therm. Sci., 12 (2008) 153–163.
[30] D. Rahul, G.N. Tiwari, Characteristic equation of a passive solar still. Desalination, 245 (2009) 246–265.
[31] H. Zurigat Yousef, K. Abu-ArabiMousa, Modeling and performance analysis of a regenerative solar desalination unit. Appl. Therm. Eng., 24 (2004) 1061–1072.
[32] A. Agrawal, R.S. Rana, P.K. Srivastava, Heat transfer coefficients and productivity of a single slope single basin solar still in Indian climatic condition: experimental and theoretical comparison, Resour.-Efficient Technol., 3 (2017) 466–482.
[33] A.E. Kabeel, Y.A.F. El-Samadony, W.M. El-Maghlany, Comparative study on the solar still performance utilizing different PCM. Desalination, 432 (2018) 89–96.
[34] V. Velmurugan, C.K. Deenadayalan, H. Vinod, K. Srithar, Desalination of effluent using fin type solar still, Energy, 33 (2008) 1719–1727.
[35] B.C. Pak, Y. Cho, Hydrodynamic and heat transfer study of dispersed fluids with submicron metallic oxide particle, Exp. Heat Transf., 11 (1998) 151–170.
[36] Y. Xuan, W. Roetzel, Conceptions for heat transfer correlation of nanofluids, Int. J. Heat Mass Transf., 43 (2000) 3701–3708.
[37] Einstein, Investigation on the theory of Brownian motion, Dover, New York, 1956.

[38] J.C. Maxwell, Treatise on electricity and magnetism, Dover, New York, 1954.
[39] K.S. Hwang, J.H. Lee, S.P. Jang, Buoyancy-driven heat transfer of water-based Al2O3 nanofluids in a rectangular cavity, Int. J. Heat Mass Transf., 50 (2007) 4003–4010.
[40] C. Popiel, J. Wojtkowiak, Simple formulas for thermo-physical properties of liquid water for heat transfer calculations (from 0oC to 50oC), Heat Transf. Eng., 19 (1998) 87–101.
[41] K. Khanafer, K. Vafai, A critical synthesis of thermophysical characteristics of nanofluids. Int. J. Heat Mass Transfer, 54 (2011) 4410–4428.
[42] A.E. Kabeel, Z.M. Omara, F.A. Essa, Numerical investigation of modified solar still using nanofluids and external condenser, J. Taiwan Inst. Chem. Eng., 75 (2017) 77–86.